Coupled Model Simulations of the West African Monsoon System: Twentieth- and Twenty-First-Century Simulations

KERRY H. COOK AND EDWARD K. VIZY

Department of Earth and Atmospheric Sciences, Cornell University, Ithaca, New York

ABSTRACT

The ability of coupled GCMs to correctly simulate the climatology and a prominent mode of variability of the West African monsoon is evaluated, and the results are used to make informed decisions about which models may be producing more reliable projections of future climate in this region. The integrations were made available by the Program for Climate Model Diagnosis and Intercomparison for the Fourth Assessment Report of the Intergovernmental Panel on Climate Change. The evaluation emphasizes the circulation characteristics that support the precipitation climatology, and the physical processes of a "rainfall dipole" variability mode that is often associated with dry conditions in the Sahel when SSTs in the Gulf of Guinea are anomalously warm.

Based on the quality of their twentieth-century simulations over West Africa in summer, three GCMs are chosen for analysis of the twenty-first century integrations under various assumptions about future greenhouse gas increases. Each of these models behaves differently in the twenty-first-century simulations. One model simulates severe drying across the Sahel in the later part of the twenty-first century, while another projects quite wet conditions throughout the twenty-first century. In the third model, warming in the Gulf of Guinea leads to more modest drying in the Sahel due to a doubling of the number of anomalously dry years by the end of the century. An evaluation of the physical processes that cause these climate changes, in the context of the understanding about how the system works in the twentieth century, suggests that the third model provides the most reasonable projection of the twenty-first-century climate.

---

1. Introduction

The purpose of this paper is to make an informed decision about which state-of-the-art coupled GCMs provide the most reliable future climate predictions over West Africa in summer, and to present projections of future climate in this region from the selected models. The ability of 18 coupled GCMs to correctly simulate the present-day climatology of the West African monsoon system, as well as the physical processes of a prominent mode of interannual variability, is used to select models that may be providing more realistic projections of future climate in this region. These GCM simulations were made available through the Program for Climate Model Diagnosis and Intercomparison (PCMDI), which enabled an unprecedented access to model integrations performed for the Fourth Assessment Report of the Intergovernmental Panel on Climate Change (IPCC). Scientists at many laboratories worldwide gave generously of their time to provide this model output.

Studies that compare climate model output often use a statistical approach to the intercomparison, sometimes combining integrations from different models to form large ensemble sets. Here, we examine and evaluate the coupled GCM output at the process level, and use this evaluation to diagnose only those models that are best suited for capturing the West African monsoon climate and its variability.

The future of the Sahel, a vulnerable region prone to long-term drought located at the northern edge of the West African monsoon system, is of special concern. Accordingly, we investigate a well-known mode of variability that associates dry conditions in the Sahel and wet conditions along the Guinean coast with the presence of warm Gulf of Guinea sea surface temperature anomalies (SSTAs). We chose to study this mode of variability for two reasons. One is its prominent influence on a vulnerable region. The other is that the physi-

Corresponding author address: Kerry H. Cook, Department of Earth and Atmospheric Sciences, Cornell University, 3114 Snell Hall, Ithaca, NY 14853.
E-mail: khc6@cornell.edu

cal mechanisms of this model are understood, so it provides an opportunity for evaluating model processes.

In the following section, background on the observed summer climatology of West Africa is provided, along with a discussion of the importance and physical processes of the dipole precipitation variability mode. Then, in section 3a, output from 18 coupled GCM simulations of the twentieth-century climate are examined to evaluate how well the models capture the northern Africa summer precipitation and circulation climatology. A subset of these simulations is selected for additional analysis of the dipole mode in the twentieth-century runs in section 3b. Based on this diagnosis, 4 twenty-first-century model integrations under various greenhouse-forcing scenarios are presented in section 4. Section 5 summarizes the conclusions.

2. Background: Climatology and variability of the West African monsoon system

Several important observed circulation features of the West African monsoon are apparent in the latitude–height cross section in Fig. 1a, which is formed using the National Centers for Environmental Prediction–National Center for Atmospheric Research (NCEP–NCAR) reanalysis climatology averaged over June–September (JJAS) for 1949–2000 (Kalnay et al. 1996). The northward low-level monsoon flow onto the Guinean coast (which is near 5°N) has maximum velocities of about 4 m s^{-1}, is confined below 850 hPa, and penetrates well onto the continent, as far north as 20°N. Much of this onshore flow feeds into the deep ITCZ convection between 5° and 10°N. The low-level flow that reaches the southern Sahara (~20°N) converges there with southward flow and rises over the continental thermal low, but this system is not as deep as the moist convective system farther south. The divergence center over the continental thermal low—the "Saharan high"—is near 600 hPa, and the meridional divergence is associated with southward velocity. The interface between the deep tropical system (~5°–10°N) and the shallower subtropical system to the north (~20°N) results in a southward tilt of the streamlines in the midtroposphere. Note the large-scale subsidence over the Gulf of Guinea south of about 2°N.

According to Fig. 1a, there are three southward wind maxima over West Africa in summer. One is close to the surface north of 20°N, where southward flow converges into the thermal low. When Coriolis forces act on this southward flow, easterly winds known as the Harmattans are formed to lift dust from the dry surface. A second southward wind maximum occurs in the midtroposphere near 15°N as part of the outflow from
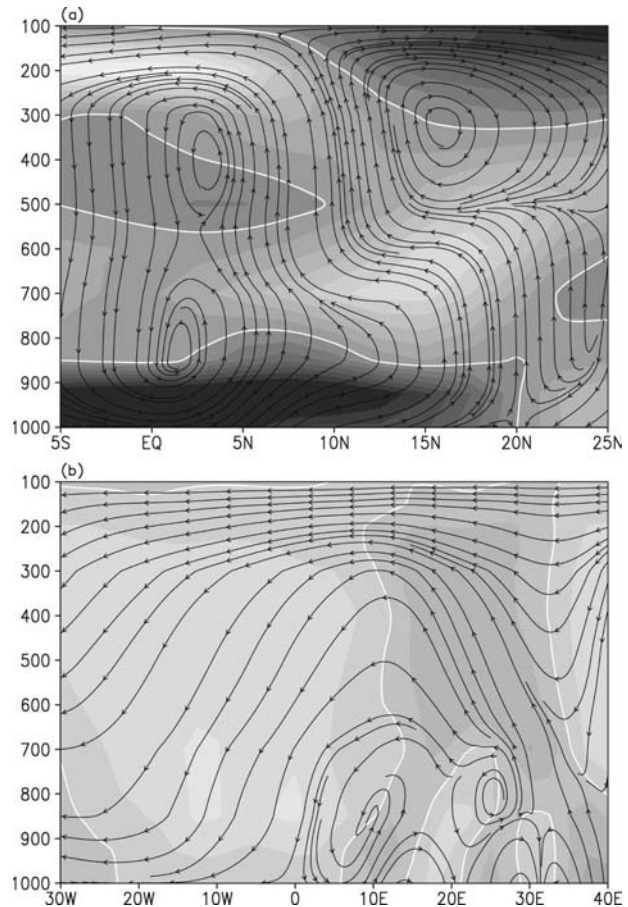

FIG. 1. (a) Latitude–height cross section of streamlines (v, $w \times 10^{-2}$) along 5°E longitude from the NCEP–NCAR reanalysis averaged over JJAS (1949–2000). Shading indicates meridional wind speeds with 1 m s^{-1} intervals. The thick white line indicates the zero meridional velocity contour, and darker shades mark positive (northward) velocity. (b) Longitude–height cross section of streamlines (u; $w \times 10^{-2}$) along 0° from the NCEP–NCAR reanalysis. Shading indicates vertical wind speeds with 0.01 m s^{-1} intervals. The thick white line denotes the zero vertical velocity contour, and darker shades mark positive (upward) velocity.

the Saharan high. Eastward Coriolis acceleration of this flow generates the African easterly jet. Similarly, southward outflow over the region of deep convection (5°–10°N) extends the tropical easterly jet near 200 hPa to the east.

The zonal circulation also places subsidence over the Gulf. Figure 1b shows streamlines, with shading to indicate vertical velocity, in a zonal cross section along the equator. There is rising motion in association with rainfall over the Congo basin, and sinking to the west over the Gulf of Guinea. Note, however, that there is no systematic return flow at low levels to complete a Walker circulation. Rather, the low-level flow diverges to the west.
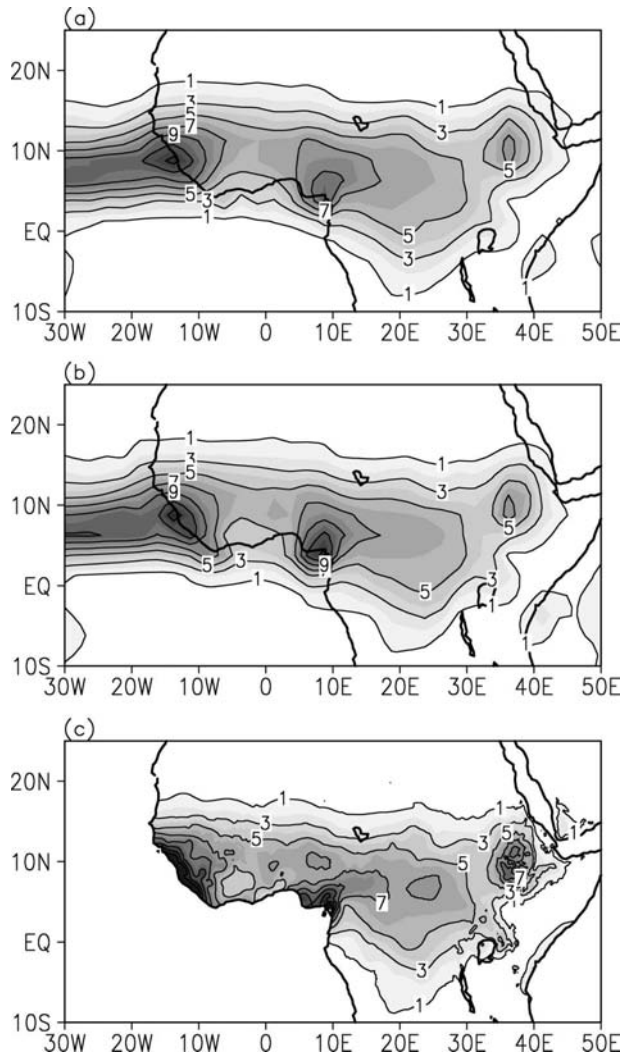
FIG. 2. JJAS precipitation (mm day^{-1}) for the (a) 1979–2003 GPCP satellite gauge 2.5° × 2.5° resolution precipitation climatology (Huffman et al. 1997), (b) 1979–2005 CPC Merged Analysis of Precipitation (CMAP) 2.5° × 2.5° resolution climatology (Xie and Arkin 1997), and (c) 1961–90 Climate Research Unit (CRU) 10-min global climate dataset (New et al. 1999). Solid lines are contoured every 2 mm day^{-1} starting from the 1 mm day^{-1} contour.

Three observational climatologies of the summer precipitation over Africa are displayed in Fig. 2. Two are constructed by blending more than 20-yr of satellite and gauge data to provide coverage over both land and ocean with a grid spacing of 2.5° × 2.5°. In both the GPCP and CMAP climatologies for JJAS, plotted in Figs. 2a,b, respectively, a zonal precipitation band is punctuated by three regional precipitation maxima. One is centered on the west coast near 8°N, another is near the Cameroon highlands in the eastern Guinean coast region, and a third appears over the Ethiopian highlands in the west. There are relative minima be-

tween 30° and 35°E in eastern Sudan, and around the Greenwich meridian near the Guinean coast. The two climatologies are very similar.

New et al. (1999) constructed a precipitation climatology using only gauge observations from 1960 to 1990, and gridded the data using 10′ spacing. This land-only climatology is shown in Fig. 2c. There is large-scale agreement with the satellite gauge climatologies (Figs. 2,b), but the precipitation maxima are larger and secondary maximum appear, for example, over southern Sudan near 7°N and 25°E.

An important mode of interannual variability in the West African monsoon system is used to evaluate the ability of the coupled GCMs to represent change in the system. This mode is prominent on interannual time scales, but it does not account for all of the variability in the West African monsoon system and is not thought to be responsible for decadal trends. It is chosen here as a way of evaluating the GCM dynamics because of its prominence, but also because the physical processes of the mode are known (see below). This provides an opportunity for a physically based analysis of the model output.

Observational studies (e.g., Nicholson 1980; Janowiak 1988; Janicot 1992; Ward 1998; Rowell et al. 1995) reveal an out-of-phase variation in rainfall between the Guinean coast (south of 10°N) and the Sahel. Nicholson and Palao (1993) suggest that this dipole pattern is one of three major spatial modes of rainfall variability over West Africa.

The dipole precipitation anomaly has been related to SSTAs in the Gulf of Guinea (Lamb 1978a,b; Hastenrath 1984; Lough 1986; Semazzi et al. 1988; Druyan 1991; Folland et al. 1991; Lamb and Peppler 1992). Janowiak (1988) correlated the first principle component for JJAS seasonal rainfall anomalies from 1927 to 1973 with the time series from Lough's (1986) second SST eigenvector for JJAS and confirmed that rainfall tends to be below normal over the Sahel and above normal along the Guinean coast when SSTAs in the southeastern Atlantic are warm. Ward (1998) related Sahelian rainfall to SSTs during dipole years, and found a significant correlation at the 95% confidence level with Gulf of Guinea SSTAs.

The dipole appears with both signs: a wet Sahel and a dry Guinean coast in association with cold Gulf of Guinea SSTAs, and a dry Sahel with a wet Guinean coast in association with warm Gulf of Guinea SSTAs. The first column in Table 1 lists those years identified as "dipole years" by Ward (1998). According to this reference, 31 of the 50 yr between 1949 and 1998 could be classified as dipole years. The second column in Table 1 indicates the state of Gulf of Guinea tempera-

TABLE 1. Identification of observed dipole years for 1949–2000.

Dipole years Ward (1998)	Gulf of Guinea SSTAs	Dipole sign (Sahel/Guinean Coast)	References*
1949	*Warm*	*Dry/wet*	*J88, J92, N00*
1950	**Cold**	**Wet/dry**	**J88, J92, N00**
1951	Warm		
1953	**Cold**	**Wet/dry**	**J88, N00**
1954	**Cold**	**Wet/dry**	**J88**
1955	Cold		
1956	**Cold**	**Wet/dry**	**J88, J92, N00**
1957	Cold		
1958	**Cold**	**Wet/dry**	**J88, J92, N00**
1960	*Warm*	*Dry/wet*	*J88, J92, N00*
1961	**Cold**	**Wet/dry**	**N00**
1963	*Warm*	*Dry/wet*	*N80, J88, J92*
1964	**Cold**	**Wet/dry**	**J88, J92, N00**
1965	Cold	Dry/wet	J88
1966	*Warm*	*Dry/wet*	*J88, J92, N00*
1967	**Cold**	**Wet/dry**	**N00**
1968	*Warm*	*Dry/wet*	*J88, J92, N00*
1969	**Cold**	**Wet/dry**	**N00**
1970	Cold	Dry/wet	J88
1973	*Warm*	*Dry/wet*	*J88*
1978	Cold		GPCP disagrees
1979	*Warm*	*Dry/wet*	*N00, GPCP agrees*
1984	*Warm*	*Dry/wet*	*GPCP agrees*
1986	Cold		GPCP disagrees
1987	*Warm*	*Dry/wet*	*N00, GPCP agrees*
1991	Warm		GPCP disagrees
1993	Cold		GPCP disagrees
1994	**Cold**	**Wet/dry**	**N00, GPCP agrees**
1995	*Warm*	*Dry/wet*	*N00*
1996	Warm		GPCP disagrees
1998	**Cold**	**Wet/dry**	**GPCP agrees**

* Janowiak (1988): J88; Janicot (1992): J92; Nicholson (1980): N80; Nicholson et al. (2000): N00; "GPCP agrees": response identifiable in the GPCP satellite gauge dataset (Huffman et al. 1997); "GPCP disagrees": response is not identifiable in the GPCP satellite gauge dataset.
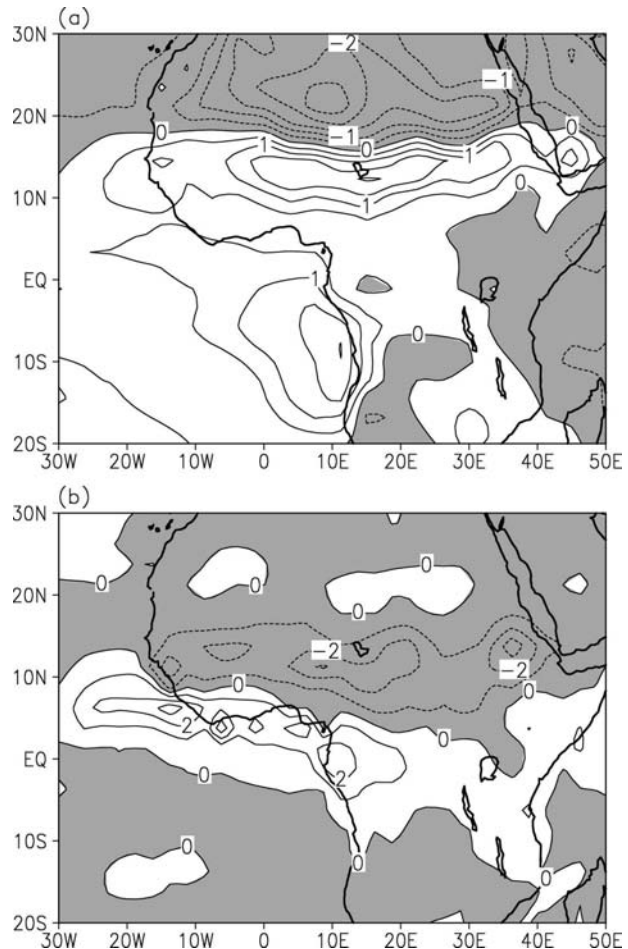

FIG. 3. The 1984 JJAS (a) NCEP–NCAR reanalysis surface temperature difference from the 1949–2000 mean, and (b) GPCP precipitation difference from the 1979–2003 mean. Contour intervals are 0.5 K in (a), and 1 mm day^{-1} in (b), with negative values shaded.

tures during each year, as indicated by an inspection of the Reynolds and Smith (1994) SST data.

Some of the years listed as dipole years by Ward (1998) are not confirmed by other studies, or by an inspection of the Global Precipitation Climatology Project (GPCP) precipitation (available after 1974). Here, to generate a count of the number of dipole years in the second half of the twentieth century, we require corroboration either from the literature or our own inspection of the GPCP precipitation. The third column in Table 1 provides information about each year's precipitation anomalies over northern Africa, and the fourth column lists the source.

By this method, we count 12 yr as having a relatively dry Sahel/wet Guinean coast precipitation anomaly in the 1949–2000 period. Of these 12 yr, 10 were accom-

panied by warm Gulf of Guinea SSTs. These years are indicated by italic font in Table 1. Similarly, there are 11 yr with the wet Sahel/dry Guinean coast dipole pattern. All of these have cold SSTAs in the Gulf of Guinea, and they are denoted by the bold font in Table 1.

The dipole pattern of precipitation is so strong that it can be seen in individual years, and not just in EOF and other statistical analyses. For example, in 1984 SSTs in the Gulf of Guinea were 0.5–1-K warmer than the 1949–2000 mean (Fig. 3a). These warm SSTs were accompanied by anomalously high precipitation north of the SSTAs, along the Guinean coast, and low precipitation across the Sahel to the north (Fig. 3b). The precipitation anomalies are on the order of 2 mm day^{-1}.

Vizy and Cook (2001, 2002, hereafter VC02) identified the physical mechanisms that connect the dipole precipitation perturbation with Gulf of Guinea SSTs.
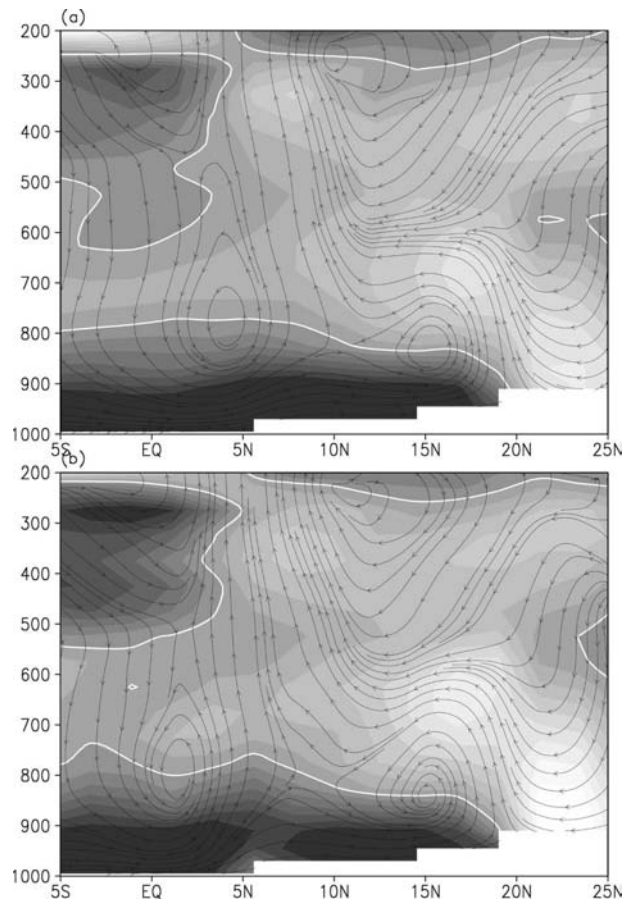
FIG. 4. (a) Latitude–height cross section of streamlines (v, $w \times 10^{-2}$) along 5°E longitude from VC02's regional climate model simulations averaged over JJAS. Shading indicates meridional wind speeds with 1 m s^{-1} intervals. The thick white line indicates the zero meridional velocity contour, and darker shades mark positive (northward) velocity. (b) Same as in (a), but when warming is imposed in the Gulf of Guinea in the model.

Figure 4a shows the meridional latitude–height cross section of the circulation from VC02's regional model simulation. Details of the observed circulation associated with the West African monsoon system (Fig. 1a) are reproduced in the simulation. When warm SSTAs are placed in the Gulf of Guinea in the regional model, the circulation changes, as displayed in Fig. 4b. The center of the monsoon circulation shifts from 6°N (Fig. 4a) to about 1°N. Because evaporation rates over the warm ocean are enhanced and the southerly flow across the Guinean coast carries more moisture, the precipitation maximum is intensified to form the positive node of the dipole over the coast. The additional midtropospheric heating in the coastal region induces stronger vertical velocities and vortex stretching. To balance the positive relative vorticity tendency in the lower troposphere forced by this stretching, the atmosphere trans-

ports additional low planetary vorticity air into West Africa across the Guinean coast, maintaining the primary Sverdrup balance that stabilizes the southern portions of the West African monsoon (Cook 1997). The response to cold Gulf of Guinea SSTAs is similar, with opposite signs and reduced precipitation over the Guinean coast countries.

This process dominates because there is subsidence over the Gulf of Guinea that suppresses convection in the vicinity of the SSTA. Thus, the precipitation anomaly maximum is north of the warm SSTAs because of the circulation induced by the presence of the African continent.

The decrease in rainfall over the southern Sahel is caused by subsidence associated with the northerly outflow from the Saharan high. A comparison between Figs. 4a,b indicates that when the Gulf of Guinea is anomalously warm, the northerly outflow from the Saharan high extends farther south. This leads to anomalous shrinking of planetary vorticity. In addition, this northerly flow occurs lower in the atmosphere, closer to 700 than 600 hPa. Since the meridional relative vorticity gradient changes sign over this vertical distance, the lower northerly flow also sinks due to shrinking of relative vorticity.

3. Evaluation of the twentieth-century coupled GCM simulations

a. Precipitation and circulation climatology

Eighteen twentieth-century integrations, some with multiple ensemble members, are examined to evaluate the accuracy with which the models can capture the West African monsoon system. Figure 5 shows JJAS precipitation averaged from 1949 to 2000 for each simulation. Table 2 provides some information about each integration, including a "short name" for each simulation, used here for convenience. The 1949–2000 time period is chosen to coincide with the period over which the dipole variability mode has been observed. All available ensemble members are averaged to form the climatology.

Each model captures the largest-scale idea of a zonally oriented precipitation maximum, but about one-third do not generate the West African monsoon (i.e., they do not bring the ITCZ and its associated rainfall onto the African continent during boreal summer). Examples include the Commonwealth Scientific and Industrial Research Organisation (CSIRO), one of the Goddard Institute for Space Studies models (GISS_ER), ECHAM5, the Community Climate System Model (CCSM), the Parallel Climate Model (PCM), and the Hadley Centre Coupled Model (HadCM) integrations.

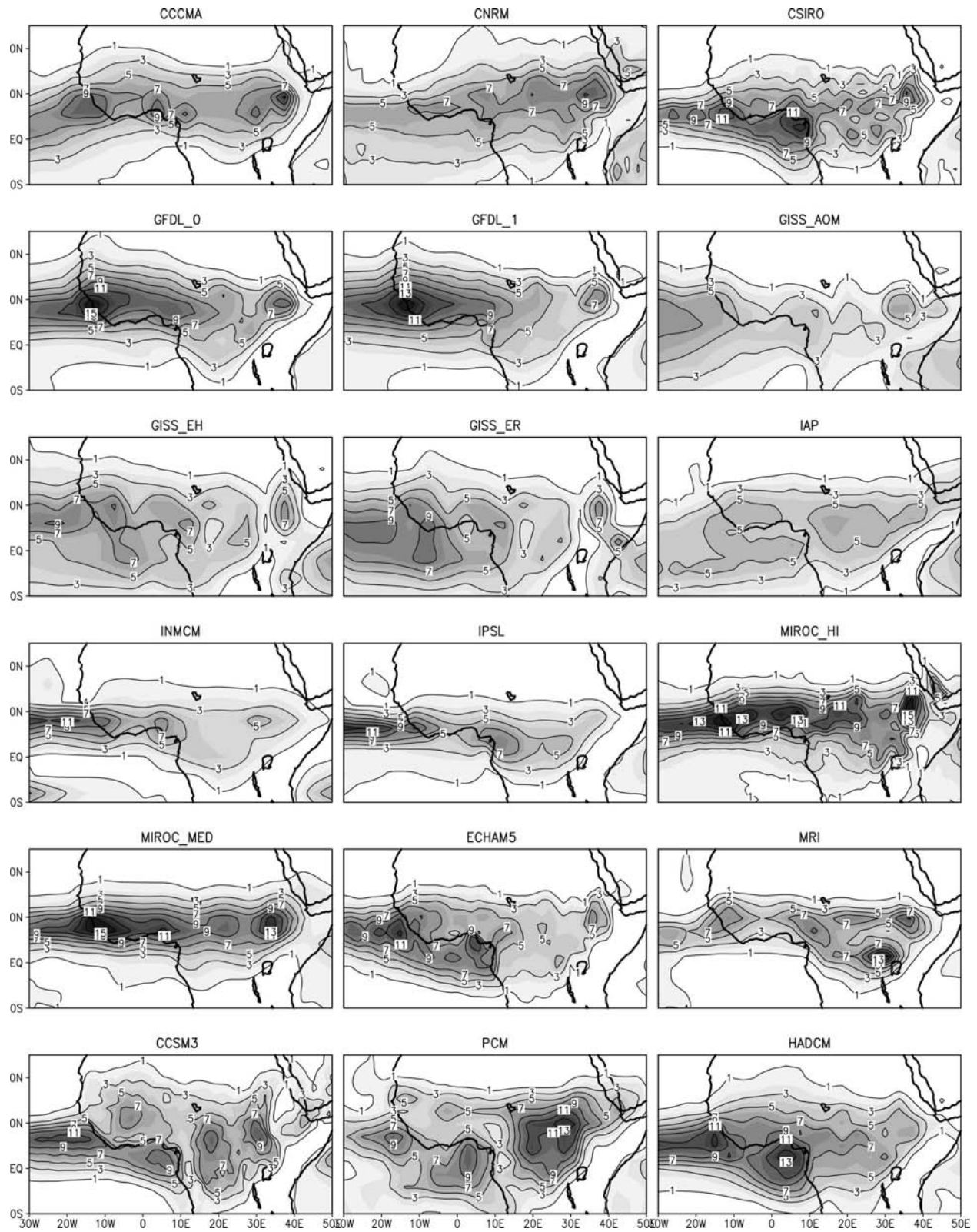FIG. 5. Simulated 1949–2000 JJAS precipitation rates (mm day^{-1}) over northern Africa from some coupled GCMs. Contours start at 1 mm day^{-1} and are every 2 mm day^{-1}; shading intervals are every 1 mm day^{-1}.

TABLE 2. Twentieth-century model integrations examined.

Integration name (IPCC model IDs*)	Short name	Grid spacing	No. of ensemble members
**CCCMA_CGCM3.1	CCCma	T47 (~3.8° lat–lon), L31	1
**CNRM-CM3	CNRM	T63 linearly reduced to T42 (~2.8° lat–lon), L45	1
CSIRO_Mk3.0	CSIRO	T63 (~1.875° lat–lon), L18	1
**GFDL-CM2.0	GFDL_0	2.0° lat × 2.5° lon, L24	3
**GFDL-CM2.1	GFDL_1	2.0° lat × 2.5° lon, L24	3
GISS_AOM	GISS_AOM	3.0° lat × 4.0° lon, L12	2
**GISS_EH	GISS_EH	4.0° lat × 5.0° lon,	5
GISS_ER	GISS_ER	4.0° lat × 5.0° lon,	9
IAP_FGOALS-g1.0	IAP	2.8° lat × 2.8° lon, L26	3
**INM-CM3.0	INMCM	4.0° lat × 5.0° lon, L21	1
**IPSL-CM4	IPSL	3.75° lat × 2.5° lon, L19	1
**MIROC3.2(hires)	MIROC_HI	T106 (~1.125 lat–lon), L56	1
**MIROC3.2(medres)	MIROC_MED	T42 (~2.8° lat–lon), L20	3
ECHAM5/MPI-OM	ECHAM5	T42 (~2.8° lat–lon), L20	3
**MRI-CGCM2.3.2	MRI	T42 (~2.8° lat–lon), L30	5
NCAR_CCSM3	CCSM	T85 (~1.4° lat–lon), L26	8
NCAR_PCM	PCM	T42 (~2.8° lat–lon), L26	4
UKMO-HadCM3	HADCM	3.75° lat × 2.5° lon	2

* Naming conventions are from the IPCC. To encourage uniformity across analyses of the IPCC integrations, these official names for each simulation are suggested online at www-pcmdi.llnl.gov/ipcc/model_documentation/ipcc_model_documentation.php.

** Indicates simulations chosen for further analysis (see text).

After the latitudinal positioning of the ITCZ, the next most prominent feature of the northern African precipitation climatology is the three precipitation maxima—on the west coast, over the eastern portion of the Guinean coast, and over the Ethiopian highlands (Fig. 2). Only the the Canadian Centre for Climate Modelling and Analysis (CCCma), GISS_EH, and the Russian Academy of Science Institute of Numerical Mathematics Climate Model (INMCM) simulations capture these three maxima over the continent, with various degrees of realism. The Centre National de Recherches Météorologiques (CNRM) model misses the west coast maximum, both Geophysical Fluid Dynamics Laboratory (GFDL) models miss the Guinean coast maximum, and L'Institut Pierre-Simon Laplace (IPSL) model severely underestimates the eastern maximum. Both the Model for Interdisciplinary Research on Climate (MIROC) simulations and the Japanese Meteorological Research Institute (MRI) insert additional maxima in similar locations to the secondary maxima in the New et al. (1999) data. ECHAM5 and HadCM capture the east–west structure of the precipitation fairly well, but off the continent.

Overall, the simulation of the northern Africa summer precipitation climatology in the current generation of coupled climate models is not nearly as realistic as the simulation of summer precipitation over North America or Europe. All of the models represented in Fig. 5 have quite reasonable precipitation magni-

tudes for North America, and the east–west precipitation gradient is captured. Meanwhile, precipitation rates on the African continent are off by an order of magnitude in a large percentage of the models, and in many place the maximum precipitation is over the ocean instead of over land. A number of factors contribute to this disparity, including the relative scarcity of observations over Africa and difficulties in representing often smaller-scale tropical precipitation systems in models.

Eight models were eliminated from the study based on the evaluation of the precipitation climatology, and the circulation was examined in the remaining 10 (indicated in Table 2). Figure 6 shows cross sections of the flow through the Greenwich meridian from these 10 integrations, for comparison with Fig. 1a from the reanalysis and Fig. 4a from the regional model.

Each of the 10 simulations captures the low-level southerly flow onto the continent because the selection excluded models that did not bring the precipitation onto the continent. But in some of the models, judging by the location of the zero line for meridional velocity, the onshore flow is either slightly deep, extending to nearly 700 hPa (as in both GFDL models and both MIROC models), or much too deep, extending well into the middle troposphere as in the CNRM and GISS_EH integrations. In all of the models selected, the low-level westerlies penetrate appropriately far north, to about 20°N.
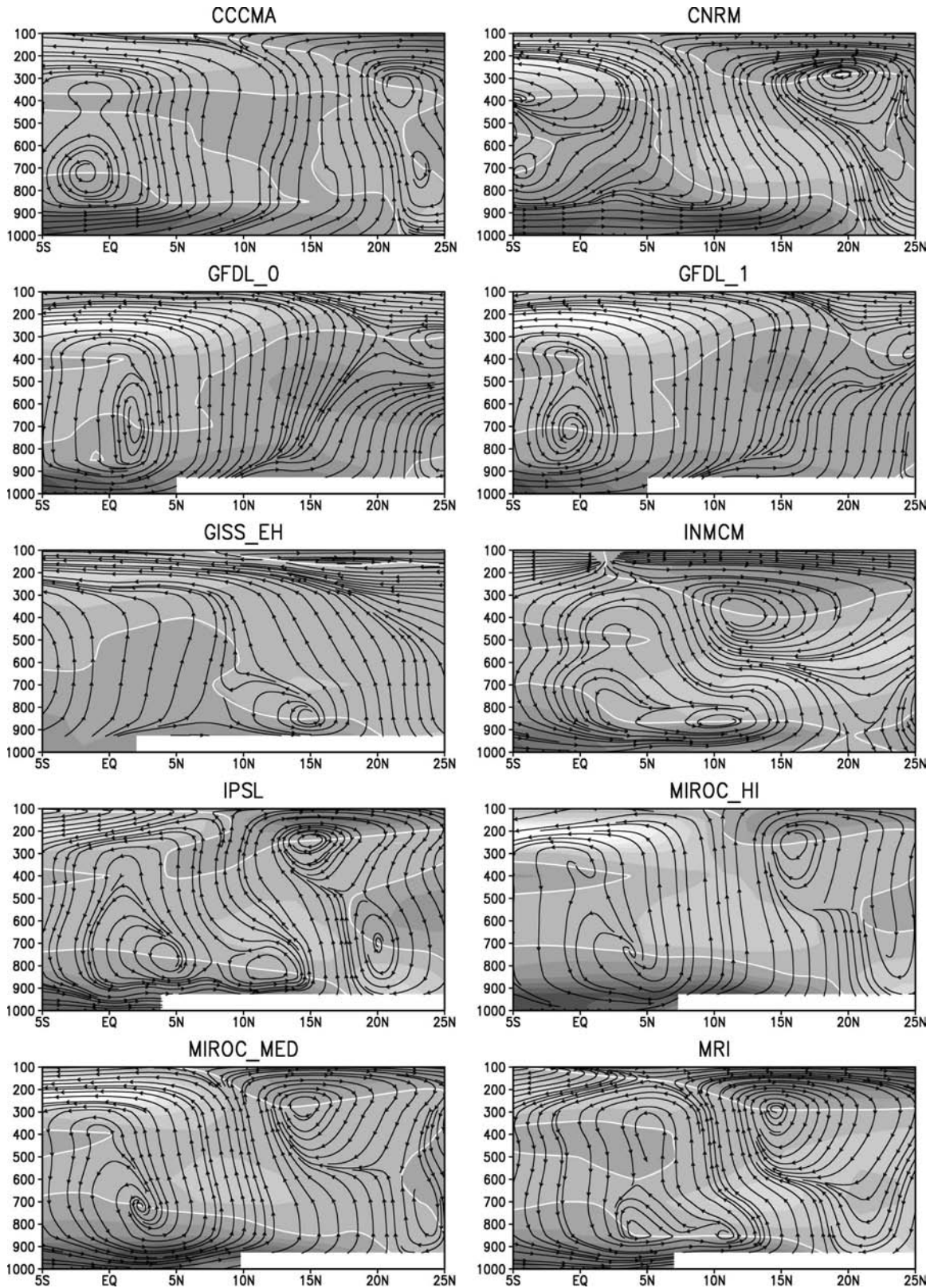
FIG. 6. JJAS streamline cross sections (v; $w_* 10^{-2}$) at 5°E in some coupled GCM integrations.

Some of the models represent the three southerly wind maxima with some accuracy, namely, CNRM, IPSL, MRI, GISS_EH, and both MIROC models. Others capture the idea of generally southerly upper-level flow but miss one or more of the maxima, such as INMCM and CCCma. Both GFDL models miss the presence of southerly flow throughout the middle and lower troposphere north of 10°N completely, with only a weak attempt at southerly flow very close to the surface north of 22°N. This occurs because the thermal low/Saharan high structure, along with its associated circulation features, is located farther east. This is a concern because placement of the thermal low too far east weakens the intense meridional gradients (in surface and low-level temperature, soil moisture, albedo, and precipitation, etc.) over West Africa.

The CCCma, CNRM, GFDL_1, and GISS models place the center of the monsoon circulation in the Southern Hemisphere and, therefore, there is rising motion instead of sinking over the Gulf. The other models simulate sinking over the Gulf, as in the observations.

In setting up their regional model simulation of northern Africa in summer, VC02 conducted a series of tests of boundary conditions and parameterizations to choose a combination that reproduces the climatology of this region with some accuracy. All of the parameterizations used are standard and widely available (see VC02 for details). In addition, these regional model simulations used a grid spacing of 120 km, comparable to those of the GCMs (see Table 2). This suggests that it is possible to capture the northern Africa summertime climatology in GCMs. It is partly just a matter of "optimizing" the model for one particular region, which can be done in a regional model. In working with a GCM, however, choices must be made considering the entire globe. Another factor explaining the disparity between the regional model and GCM simulations is that the VC02's regional model was an atmosphere-only model, forced by realistic SSTs. However, it is not clear that atmosphere-only GCM simulations have a more realistic representation of the West African monsoon than these coupled models (Gadgil and Sajani 1998).

b. Ability of the selected GCMs to capture the precipitation dipole response

To evaluate the degree to which the selected model integrations capture the dipole pattern in the twentieth-century integrations, the models' SST variability in the Gulf of Guinea is first examined. One cannot expect that a coupled GCM would reproduce specific observed warm years in the Gulf of Guinea, but the SSTAs

should have reasonable frequencies and magnitudes when compared with the observations.

Figure 7 (top) displays SSTAs in the Gulf of Guinea from Reynolds and Smith (1994) as gridded in the NCEP–NCAR reanalysis. The annual anomalies are differences between the mean JJAS SSTs in the Gulf (5°S–4°N, 5°W–5°E) for an individual year and the 1949–2000 JJAS mean for the same region. Note that there is no trend in Gulf of Guinea SSTs during this time. (The dipole variability mode is not implicated in the decadal-scale drying in the Sahel.) The average SSTA magnitude is 0.44 K.

Gulf of Guinea temperatures and SSTAs in the coupled GCMs are also displayed in Fig. 7. Anomalies are calculated relative to each simulation's Gulf of Guinea mean temperature. When more than one ensemble member is available, only one is used since averaging over more than one may dampen the anomalies and give an artificially low estimate of the SST forcing.

All of the modeled Gulf of Guinea mean SSTs are warmer than the observations by amounts ranging from approximately 0.5 K (MRI) to nearly 3 K (GISS_EH). Some of the models [CNRM, MRI, CCCma, MIROC(hires)] have warming trends in the Gulf of Guinea through the second half of the twentieth century, unlike the observations.

The magnitude of the SSTAs is somewhat subdued in some of the simulations [e.g., IPSL, MIROC(medres), MRI]. Both GFDL models produce anomaly magnitudes that are greater than those observed.

To test for the presence of the dipole variability mode in the models, summer precipitation anomalies were averaged over the Sahel (10°–15°N, 10°W–10°E) and the Guinean coast region (4°–9°N, 10°W–10°E). The signs of the anomalies in these two regions were compared, and the numbers of years in which the signs were opposite were counted and listed in Table 3. Then, the signs of the SSTAs in the Gulf of Guinea were calculated for the years with dipole precipitation anomalies, and the percentage of years with both a dry Sahel/wet coast (wet Sahel/dry coast) and a warm (cool) Gulf of Guinea were noted in the table.

Some of the coupled models produce a large number of years in which a dry Sahel/wet coast is accompanied by warm Gulf of Guinea SSTAs, similar to the observations. Both GFDL models and the GISS_EH simulations, for example, capture this association. MRI also captures this mode of variability, but one ensemble member has only 45% of the dry/wet years associated with warm SSTs. (Since SSTAs are defined as either warm or cold, this means that 55% of the dry/wet years are associated with cold SSTs.) MIROC(medres) has
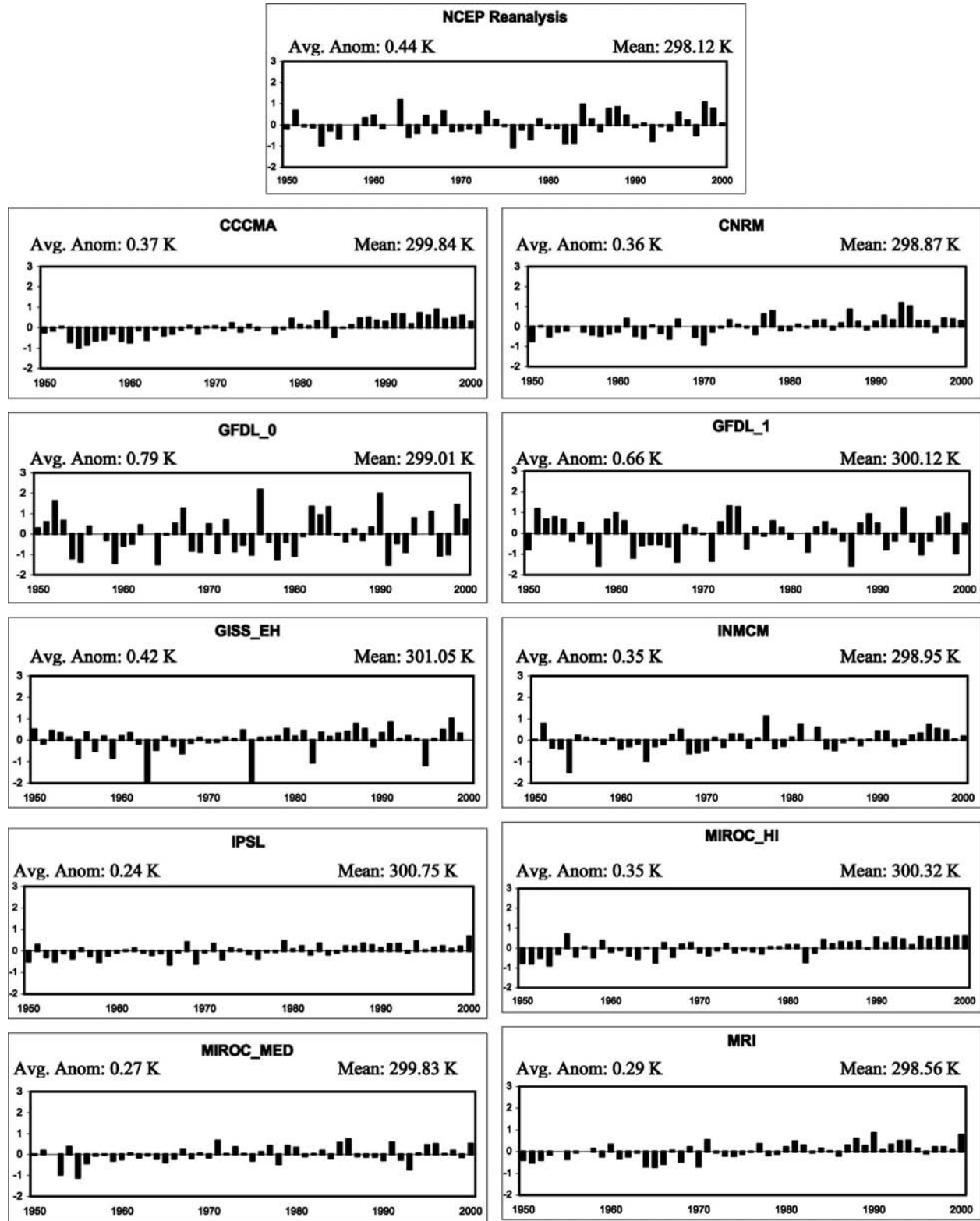
FIG. 7. JJAS SSTAs (K) in the Gulf of Guinea, calculated as deviations from each model's 1949–2000 mean over the region 5°S–4°N, 5°W–5°E. Mean SSTs for this region, and the average magnitude of the anomalies, are noted for each simulation.

TABLE 3. Occurrence of the precipitation dipole in observations and coupled GCM integrations for 1949–2000.

Source		No. of years with dry Sahel/wet coast summers	No. (%) of dry/wet summers with warm SSTAs	No. of years with wet Sahel/dry coast summers	No. (%) of wet/dry summers with cold SSTAs
Observations/reanalysis		12	83%	11	100%
CCCma		*13*	*39%*	*9*	*78%*
CNRM		*10*	*40%*	*12*	*50%*
GISS_EH	1	13	85%	10	80%
	2	10	90%	11	64%
	3	7	86%	9	78%
	4	14	71%	11	55%
	5	8	88%	10	80%
	Mean	*10*	*84%*	*10*	*71%*
GFDL_0	1	14	71%	15	93%
	2	12	75%	15	87%
	3	17	88%	15	73%
	Mean	*14*	*78%*	*15*	*84%*
GFDL_1	1	14	71%	13	62%
	2	9	78%	15	40%
	3	9	100%	11	55%
	Mean	*11*	*83%*	*13*	*52%*
INMCM		*12*	*58%*	*5*	*60%*
IPSL		*11*	*55%*	*5*	*20%*
MIROC_HI		*13*	*69%*	*14*	*50%*
MIROC_MED	1	12	83%	12	67%
	2	15	60%	15	60%
	3	10	50%	11	64%
	Mean	*12*	*64%*	*13*	*64%*
MRI	1	9	78%	11	73%
	2	9	67%	9	67%
	3	11	82%	11	82%
	4	12	42%	15	87%
	5	12	67%	14	86%
	Mean	*11*	*67%*	*12*	*79%*

a fairly wide spread among the ensemble members. Other models (CCCma, CNRM, INMCM, and IPSL) do not regularly associate warm Gulf of Guinea SSTAs with the dry Sahel/wet coast precipitation pattern.

The models that associate warm Gulf of Guinea SSTAs with the dry Sahel/wet coast pattern tend to also associate cool Gulf of Guinea SSTAs with the opposite precipitation pattern. One exception is the CCCMA model, which has a 78% percentage for the cool SSTA case, but only 39% for the warm case. Another exception is GFDL_1, which captures the warm SSTA case, but not the cool SSTA case.

The record length (1949–2000) is too short to permit a trustworthy statistical analysis, but more years cannot be included because a longer observational record of the dipole mode is not available. However, since the dynamics of this mode of variability is known, further evidence for the presence of the dipole mode in the models can be found by considering the form of the precipitation, SST, and circulation anomalies.

At this point, two models are dropped from the study. Even though the two GFDL models list significant differences in parameterizations, they produce similar results over northern Africa in summer, both in terms of the climatology and the dipole mode. Therefore, only one is analyzed here, namely, GFDL_0. (Since this is a process-oriented study, combining the output from the two GFDL models that may be behaving differently would confound the analysis.) In addition, the dynamics of the dipole in the MIROC(hires) model is not analyzed. We also concentrate on the dipole anomaly with warm Gulf of Guinea SSTAs, since this sign is more relevant for the future and of greater impact for humans.

A composite representation of the dipole mode with warm SSTAs is constructed by averaging JJAS precipitation anomalies in which the dry Sahel/wet Guinean coast precipitation dipole pattern appears accompanied by warm Gulf of Guinea SSTAs for each simulation retained. (The number of dipole years averaged for each model is indicated in the third column of Table 2.) When more than one ensemble member is provided in
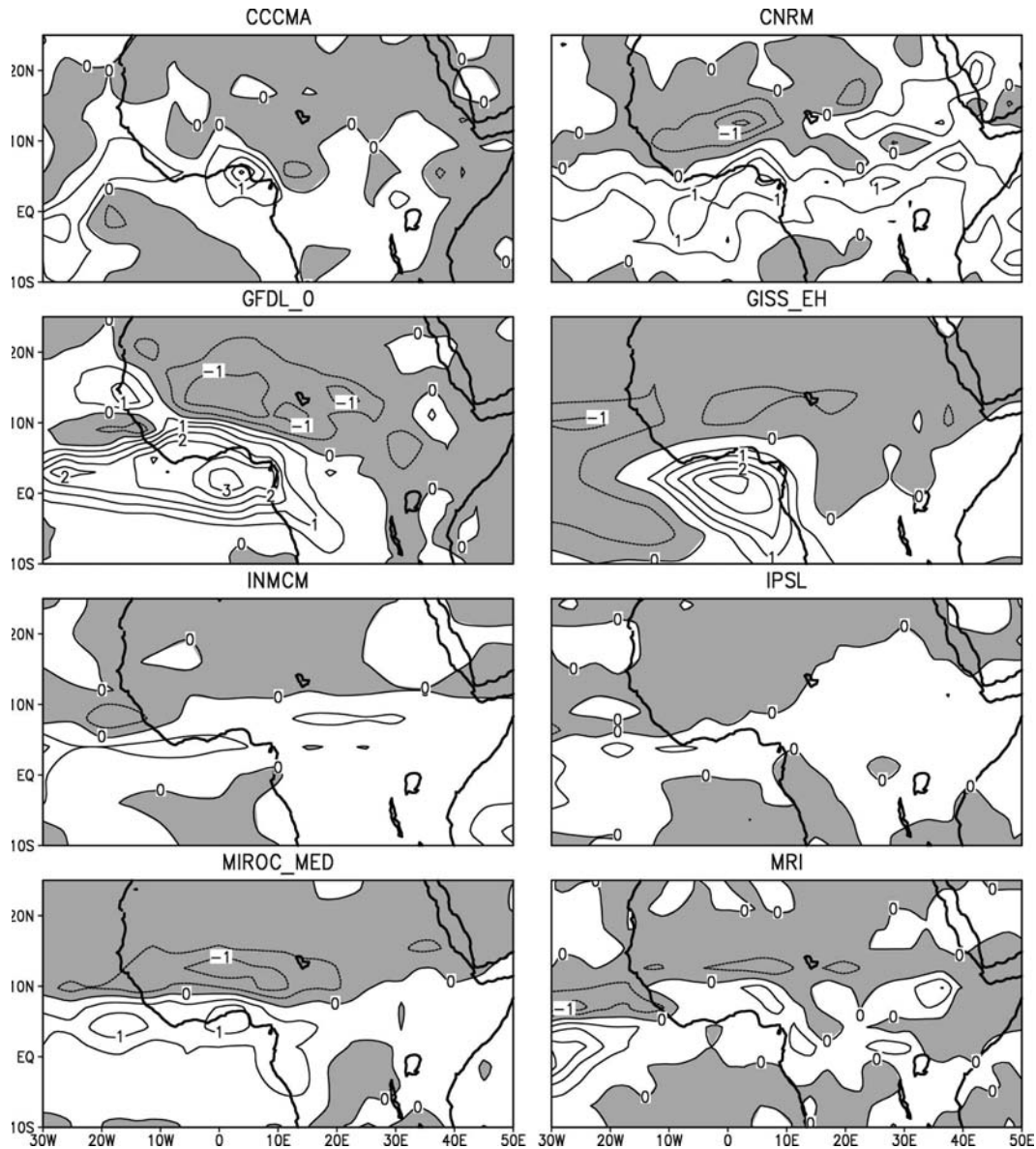
FIG. 8. Dipole-year composites of summer precipitation from various GCM integrations, differenced from the 1949–99 summer climatology produced in each model. Contour intervals are every 0.5 mm day^{-1}, and shading denotes negative values.

the PCMDI database, only member 1 is used in forming the composite.

Composite precipitation anomaly distributions are shown in Fig. 8. The negative pole of the dipole anomaly over the Sahel is much weaker than the positive pole in several models (CCCma, GISS_EH, INMCM, and IPSL). This is reminiscent of the GCM study of Vizy and Cook (2001), who noted than the northern part of the dipole seems to be more difficult to capture in global models, perhaps because so many features of the northern Africa climatology need to be in

place in the simulation to capture the dynamics of this part of the response (see section 2).

The GFDL_O and GISS_EH simulations, in which nearly all of the dry Sahel/wet Guinean coast years are accompanied by warm Gulf of Guinea SSTAs, exhibit a very strong wet signal over the northern part of the Gulf of Guinea that extends unrealistically into the Southern Hemisphere. In the CNRM and MIROC(medres) models, the magnitude of the precipitation anomaly is similar to that in the observations and the regional model process study, and in the rest of the
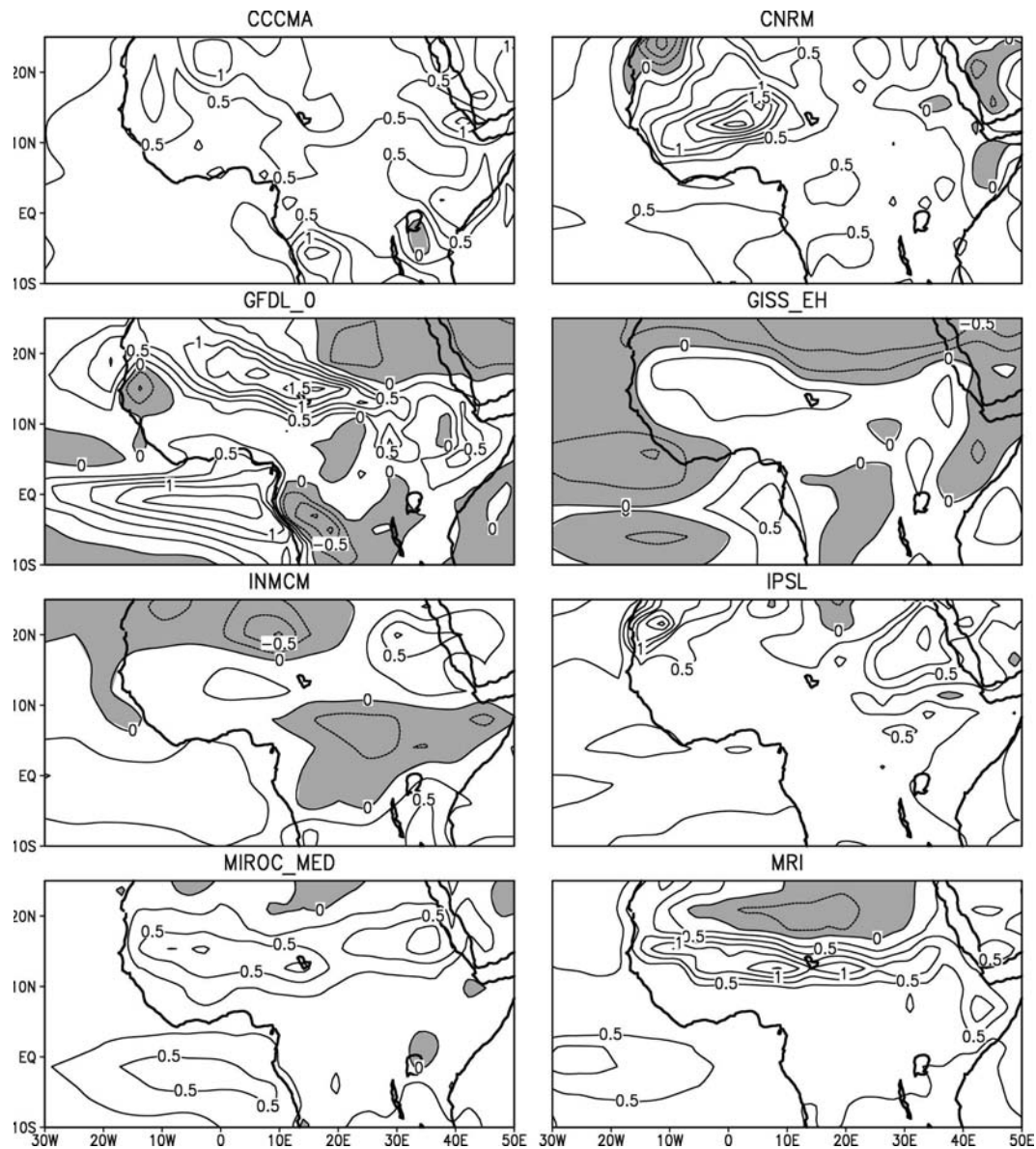
FIG. 9. Same as in Fig. 8, but for summer surface temperature from coupled GCM integrations. Contours are every 0.25 K, and shading denotes negative values.

models the precipitation anomalies are somewhat weak.

One possible reason for a strong or weak dipole response in a model is a strong or weak SSTA in the Gulf of Guinea. Composite surface temperatures, formed by averaging the same years as the precipitation composites in Fig. 8, are shown in Fig. 9. The warm SSTAs that are associated with the dipole response in most of the models are quite weak, similar to or weaker than the 1984 observations (Fig. 1). An exception is the GFDL_0 model, which produces Gulf of Guinea SSTAs that are larger, and that also seem to be cen-

tered symmetrically about the equator (also see Fig. 7). Unlike the GFDL_0 model, the strong wet anomaly in the Guinean coast region in the GISS_EH model is associated with a fairly weak warm SSTA.

The process study with the regional model discussed above suggests some basic features of the circulation that should accompany the dipole mode. Dipole composites from each model are examined for evidence of three features accompanying the dipole.

First, the precipitation enhancement should be north of the Gulf of Guinea SSTA, since one prominent feature of the dynamics of the dipole response is that sub-

sidence over the Gulf of Guinea inhibits convection there and prohibits the formation of a precipitation anomaly over the warm SSTA. As seen by comparing Figs. 8 and 9, some of the simulations place the positive precipitation anomaly clearly north of the SSTA, such as the CCCma and MIROC(medres) models. In the GFDL_0 and GISS_EH models, the maximum precipitation anomaly is north of the SSTA by a few degrees of latitude.

Second, the composite meridional circulation is examined for evidence of a southward shift of the monsoon circulation compared with the climatology. This is not generally a feature of the dipole precipitation anomaly in the GCM simulations (not shown). The center of the monsoon circulation in the composites is located farther south in only two of the models: GFDL_0 and CNRM.

The third feature also concerns the meridional circulation, and the composites are examined for evidence of southward wind anomalies in the midtroposphere in association with the dipole. A negative precipitation anomaly over the Sahel due to some other reason could cause such an anomaly, of course, and cause and effect cannot be distinguished by examining a climatology. However, the regional model process study implicates southerly wind anomalies north of the Sahel precipitation anomaly in inducing subsidence through shrinking of absolute vorticity.

Differences between the dipole composites and the climatology for the meridional wind on the Greenwich meridian for each coupled model simulation are displayed in Fig. 10. Only one model, INMCM, does not generate southerly wind anomalies in the midtroposphere north of the region of drying during dipole events.

Table 4 summarizes these dynamical features of the dipole variability mode in the models under consideration. The dipole mode is captured in four of the simulations [GFDL_0, GISS_EH, MIROC(medres), and MRI], and in each of these southward midtropospheric wind anomalies accompany dry conditions in the Sahel and the maximum precipitation anomaly is to the north of the SSTA. However, none represents the southward shift of the center of the monsoon circulation as observed in the regional model process study of VC02. It is quite possible that this shift is not necessary for the formation of the dipole, if the southerly wind anomaly can form in its absence.

4. The future of the West African monsoon system in coupled GCMs

The coupled models that were selected above for their ability to capture the region's climatology and the one mode of variability are now examined under various assumptions about how greenhouse gas levels will change in the future.

Many of the coupled GCMs were run with seven or eight different scenarios for future anthropogenic emissions of CO_2, CH_4, N_2O, and SO_2. Here, simulations under four forcing scenarios are examined, known as "COMMIT," "A1B," "A2," and "B1." The COMMIT scenario freezes emissions at 2000 levels during the twenty-first century. The A1B and A2 scenarios assume similarly steep CO_2, CH_4, and SO_2 increases during the first decades of the twenty-first century. These emissions start to decline in the A1B scenario before 2050, while strong increases in emissions are maintained throughout the century in the A2 scenario (except for SO_2, which declines after 2030). There are small increases in emissions through the early decades of the twenty-first century in the B1 scenario, with declining emissions after about 2040. [More details about these scenarios are available in the IPCC Third Assessment Report (TAR; Houghton et al. 2001)].

Output from the GFDL_0, MRI, and MIROC(medres) models for each of these scenarios is available, with one, three, and five ensemble members, respectively. At the time of writing, the GISS_EH model only had twenty-first-century simulations available for the A1B scenario, with three ensemble members.

Table 5 lists the numbers of years in which both signs of the precipitation dipole pattern appear in future climate simulations with the fours models. All available ensemble members are included, and the criteria for identifying the dipole pattern are the same as for the twentieth-century integrations. No attempt is made to associate these precipitation patterns with SSTAs in the Gulf of Guinea since all of the models in virtually every case (except a few scattered years in the COMMIT scenario) simulate a warming trend in the Gulf of Guinea throughout the twenty-first century (see below). In the presence of such a temperature trend, it does not make sense to talk about temperature anomalies in the same way as for the twentieth-century observations and integrations, which have no trend in the Gulf of Guinea.

The GFDL_0 and MRI models generate many more dry/wet precipitation years, and less wet/dry years, in each of the four twenty-first-century integrations examined (Table 5). But in the GFDL_0 simulations, the number of dipole events does not increase with the severity of the scenarios (e.g., there are less dry/wet dipole events in the A2 case than in the B1 case). This is a clue that the model is not producing the dipole signal in the latter part of the century (see below). With five ensemble runs available for the A2 and B1 sce-
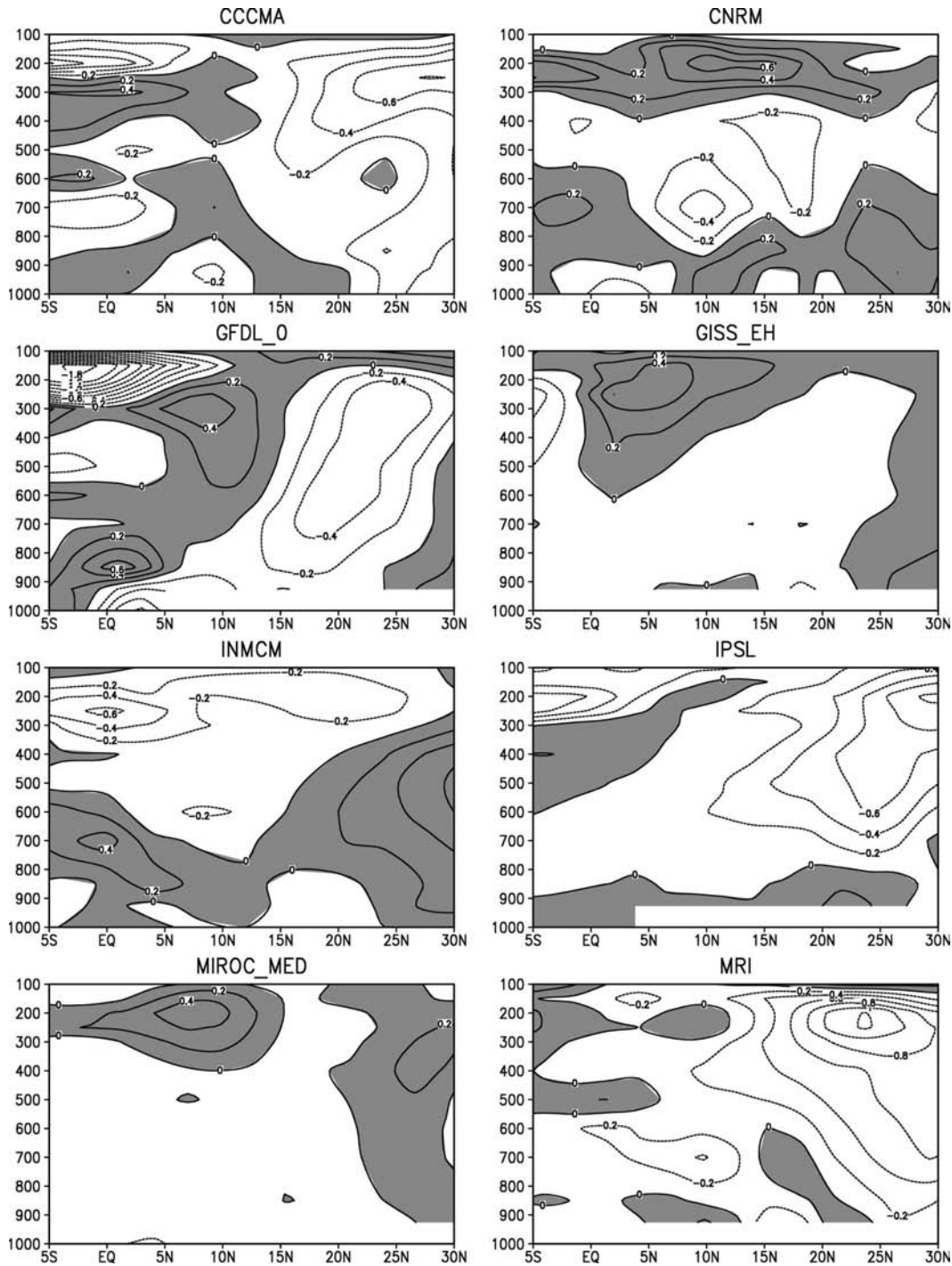
FIG. 10. Same as in Fig. 8, but for summer meridional velocity at 5°E from coupled GCM integrations. Contours are every 0.2 m s^{-1}, and shading denotes negative values.

narios, a correlation between the severity of the scenario and the numbers of dipole events in the MRI simulations is evident.

The first ensemble from the GISS_EH A1B simulations is similar to the GFDL_0 and MRI simulations in

generating more dry/wet dipole events and less wet/dry events. However, the other two members have reduced numbers of both events.

The MIROC model exhibits a huge increase in wet/dry events in all of the twenty-first-century runs and a

TABLE 4. Presence of features of the dipole dynamics in the coupled GCMs.

Source	Dipole present? (>70%)	Precipitation anomaly north of SSTA?	Southward monsoon shift?	Anomalous midtropospheric southerlies north of negative precipitation anomaly?
CCCma	No	Yes	No	Yes
CNRM	No	Maybe	Yes	Yes
GISS_EH	Yes	Yes	No	Yes
GFDL_0	Yes	Slightly	Yes	Yes*
INMCM	No	Yes	No	No
IPSL	No	No	No	Yes
MIROC_MED	Yes	Yes	No	Yes
MRI	Yes	Yes	No	Yes

* This model does not have climatological southerly flow in this region, so the southerly anomaly weakens the westerlies.

sharp decrease in dry/wet events. The wet conditions over the Sahel are stronger in the severe A2 scenario than under the milder B1 assumptions.

Because of the availability of multiple ensemble members in two of the models, and because the severity of the emissions assumptions provides a strong signal to

TABLE 5. Occurrence of the precipitation dipole in observations and coupled GCM integrations for various twenty-first-century scenarios.

	Source		No. of years with dry Sahel/ wet coast	% of twentieth-century dry/wet years*	No. of years with wet Sahel/dry coast	The % of twentieth-century wet/dry years*
Model	Scenario	Ensemble				
GFDL_0	A2	1	34	126%	10	34%
	A1B	1	33	123%	7	24%
	B1	1	41	152%	6	21%
	COMMIT	1	35	130%	17	59%
GISS_EH	A1B	1	35	137%	9	46%
		2	10	39%	16	82%
		3	18	71%	6	31%
		Avg	21	82%	10	53%
MIROC(medres)	A2	1	2	9%	68	296%
		2	6	26%	70	304%
		3	1	4%	72	313%
		Avg	3	13%	70	304%
	A1B	1	1	4%	67	291%
	B1	1	5	22%	57	248%
		2	8	35%	61	265%
		3	9	39%	55	239%
		Avg	7	32%	58	251%
	COMMIT	1	15	65%	31	135%
MRI	A2	1	42	242%	2	9%
		2	25	134%	4	19%
		3	32	185%	4	19%
		4	34	197%	7	33%
		5	46	266%	6	28%
		Avg	36	205%	5	22%
	A1B	1	27	156%	6	28%
	B1	1	21	121%	3	14%
		2	22	127%	6	28%
		3	20	116%	14	66%
		4	29	168%	9	42%
		5	23	133%	6	28%
		Avg	23	133%	8	36%
	COMMIT	1	31	179%	10	47%

* Relative to the prorated number of events in the twentieth-century integrations.
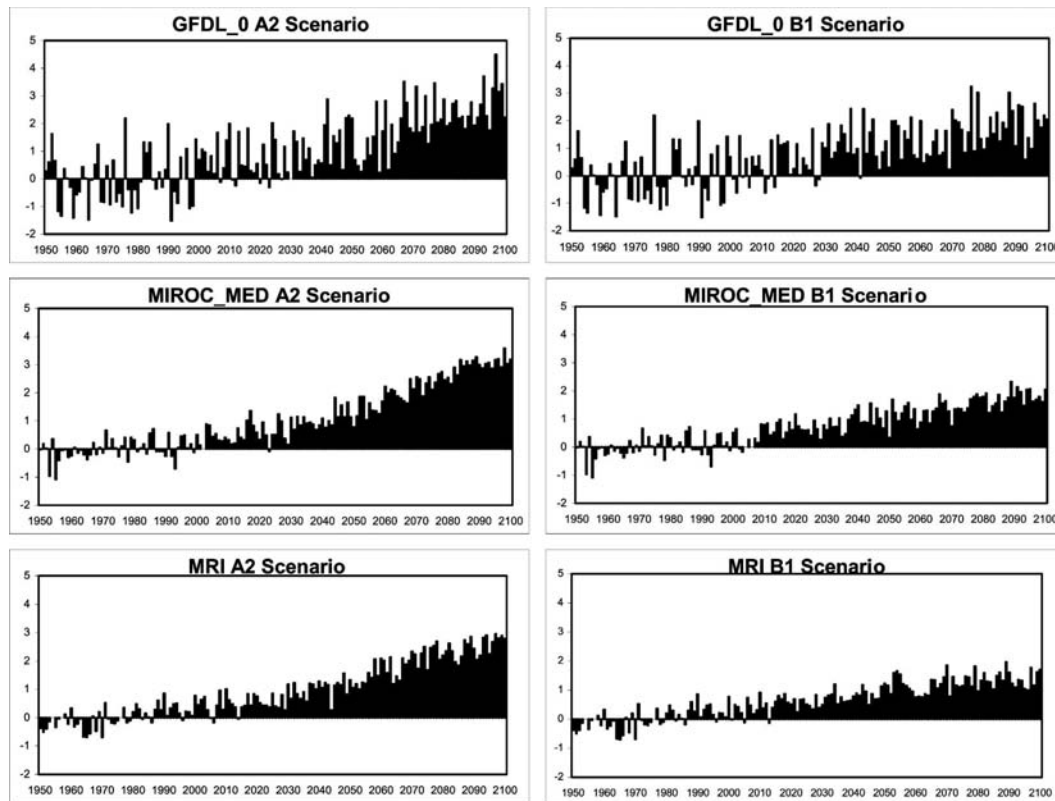
FIG. 11. JJAS Gulf of Guinea SST anomalies (K) for various GCM integrations, calculated as the difference from the 1949–2000 mean in each model. Values from simulations with the (left) A2 scenario forcing and (right) the B1 forcing are shown.

analyze, simulations under the A2 assumptions are examined in more detail. Then, the results for the second half of the twenty-first century under the A2 and B1 assumptions are compared to understand whether or not reducing emissions changes the prediction. Unfortunately, this choice eliminates the GISS_EH simulations from further analysis.

Figure 11 shows how JJAS mean SSTs in the Gulf of Guinea change in the twenty-first-century runs under the A2 and B1 scenarios in the GFDL_0 simulation, and in ensemble member 1 in the MIROC(medres) and MRI simulations. The second half of the twentieth century is included for perspective. GFDL_0 continues to have a high level of interannual variability, as in the twentieth-century runs. Under both scenarios, in all three models, the Gulf of Guinea warms in the twenty-first century. The magnitude of the SST warming is about twice as large in the A2 runs as in the B1 runs in the second half of the century. The magnitudes of the SSTAs are greater than 1 K by about 2020. Since SSTAs of this magnitude generate the dipole response in the twentieth-century climate (e.g., Fig. 3), these results suggest that changes in West African precipitation

may occur within the next two or three decades due to greenhouse gas increases.

The left-hand panel in Fig. 12 shows precipitation rates averaged over the Guinean coast region through the twenty-first century in the GFDL_0, MIROC(medres), and MRI twenty-first-century integrations under the A2 scenario forcing. In the presence of warming in the Gulf of Guinea (Fig. 11), rainfall along the Guinean coast will increase if the dynamics described above dominates (i.e., if subsidence over the Gulf of Guinea is maintained and the flow continues to have a northward component). However, both the GFDL_0 and MIROC(medres) simulations generate drying in this region later in the century. (The twenty-first-century dipole events in the GFDL_0 simulation were in the first half of the century.) In the GFDL_0 model, the drying becomes established in the later half of the century. In the MIROC(medres) model, the region becomes suddenly dry right at the beginning of the twenty-first century. Precipitation trends are not in evidence—the models just start producing a long string of dry years that maintain a similar magnitude through the years.
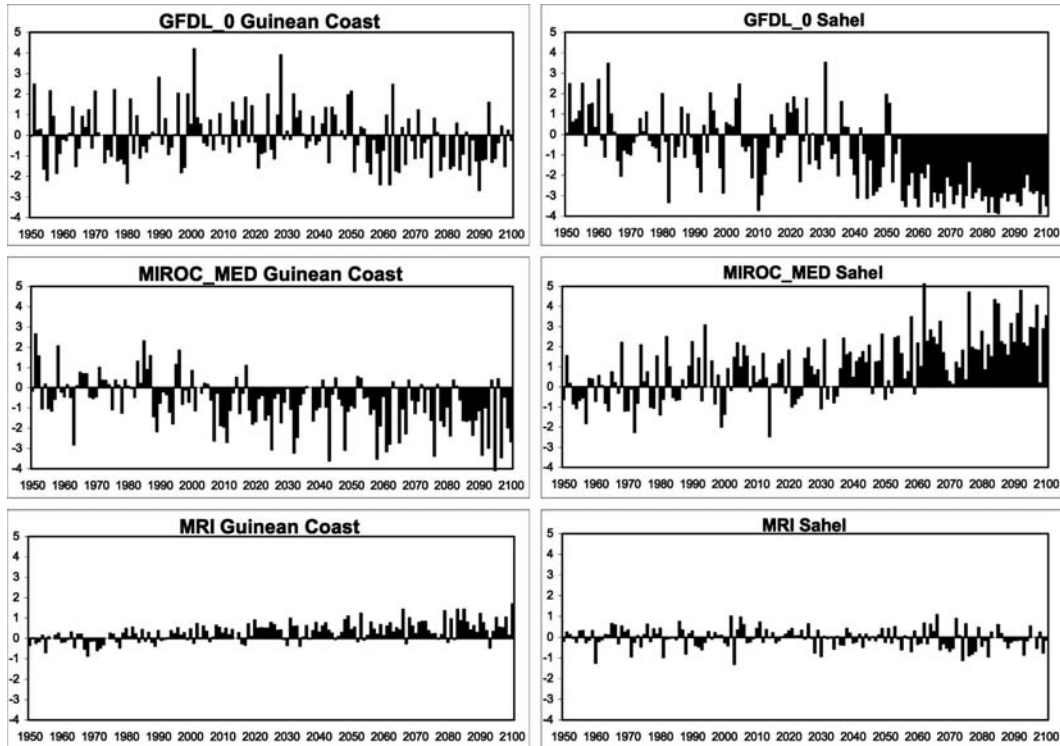
In the MRI model, Guinean coast precipitation rates

FIG. 12. (left) Guinean Coast JJAS precipitation differences (mm day^{-1}) from the 1949–2000 mean in various GCM simulations with A2 scenario forcing after 2000. (right) Sahelian JJAS precipitation differences (mm day^{-1}) from the 1949–2000 mean in various GCM simulations with A2 scenario forcing after 2000.

gradually increase through the century. In this model, which produces a warming trend in the Gulf of Guinea throughout the second half of the twentieth century (Fig. 11), the precipitation trend in the twenty-first century is a continuation of the twentieth-century trend. These precipitation increases are consistent with the dynamics of the dipole variability mode.

The Sahelian precipitation time series for the same three models under the A2 forcing is shown in the right-hand panel in Fig. 12. Rainfall rates decline sharply throughout the twenty-first century in the GFDL_0 simulation, and their decline precedes the onset of the precipitation decreases along the Guinean coast. This is not the dipole variability mode. Rather, there is a strong drying in the Sahel due to some other cause that strengthens and spreads south through the century, weakening and displacing the entire West African monsoon system in this model by about 2050. (This is the only model of the 18 models listed in Table 2 that behaves this way.)

MIROC(medres) chooses another path, and the Sahel becomes quite wet after about 2030, after dry conditions have become established in the Guinean coast region. This is also not the dipole variability mode, since the Gulf of Guinea is warm.

Unlike the GFDL_0 and MIROC(medres) models, the MRI model behaves in a way that is consistent with the dynamics of the precipitation dipole. As the twenty-first century progresses and the Gulf of Guinea warms (Fig. 11), there are more dry summers in the Sahel. The occurrence of these dry years is not as regular as the wet years to the south (Fig. 12). This is consistent with our understanding about how well the dipole dynamics is captured in GCMs, since it seems to be more difficult for the models to capture the northern part of the signal than the southern part (see section 2 and VC02). Again, Sahelian drying does not express itself as a regular trend, but as an increase in the frequency of dry years. This is similar to the result by Meehl and Tebaldi (2004), derived from model simulations, that there may be more frequent heat waves in North America and Europe under greenhouse gas forcing.

The MRI model simulates a sequence of especially dry years between 2065 and 2079, but these do not seem to be accompanied by especially wet years over the Guinean coast as might be expected from the dipole dynamics. However, an examination of the individual years (not shown) demonstrates that the dipole pattern occurs in 7 of these 15 yr. The averaging regions were chosen by examination of the observed dipole pattern,

and are used consistently for all of the 18 models in present-day and future simulations to make the evaluation more objective. In the case of the MRI mode for these seven dipole years, the area averaging is not capturing the magnitude of the precipitation anomaly accurately, but the signs are correct and the dipole pattern is produced.

It is clear from an examination of these coupled GCM simulations that there is no consensus among the models concerning the future of the West African monsoon system under greenhouse gas forcing. Consensus can often be used to build confidence in model predictions, but that option is not available in this case. Rather, as discussed above, our understanding of the West African monsoon climatology and its variability can be used to evaluate the accuracy and reliability of the simulations for the West African monsoon. Therefore, the dynamics of the response in each of the three selected simulations is examined to understand how well these responses relate to how the West African monsoon system works, and varies, in the present-day climate. The goal is to examine the workings of the system at the process level, and to defend the selection of those simulations that provide the best prediction of future climate.

The examination of the twentieth-century integrations of the GFDL models (both GFDL_0 and GFDL_1) revealed a flaw in the simulation of the climatological meridional circulation along the Greenwich meridian—a failure to produce southward flow in the midtroposphere (outflow from the Saharan high) over the western Sahel (Fig. 6). In the second half of the twenty-first century in the A2 (A1B and B1) scenarios, however, pronounced surface warming (over 7 K) develops north of 15°N, and GFDL_0 produces a circulation over the Sahel that is more similar to today's climate, with low-level convergence into the thermal low and outflow (mainly northerly and easterly) near 600 hPa near the Greenwich meridian. However, the resulting strong surface temperature gradients generate an extremely strong African easterly jet over West Africa that diverges moisture to the west below the level of condensation. This moisture divergence helps maintain the very dry conditions over all of West Africa, including the Guinean coast, in this model in the twenty-first-century integrations.

It is not possible to determine cause and effect by examining the climatology, since the fields are mutually adjusted, and a fuller understanding of this extreme drying response would require process and sensitivity studies with the model.

The precipitation anomaly that develops in the MIROC(medres) simulation, with wetter conditions in
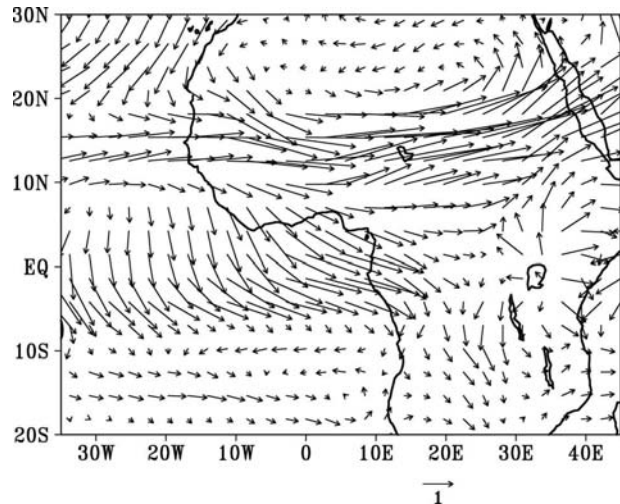

FIG. 13. JJAS differences in the 850-hPa flow between the 2071–2100 A2 scenario mean and the 1949–2000 mean from the MIROC(medres) simulations. Vector scale is in m s^{-1}.

the Sahel and drying along the Guinean coast, is related to strong warming localized in the Gulf of Guinea. In the last 20 yr of the twenty-first century, Gulf of Guinea SSTs have warmed to 304 K, and geopotential heights over the Gulf of Guinea fall below those of the land surface to the north. This reversal of the meridional height gradient breaks the monsoon, and generates a southward flow anomaly along the Guinean coast (Fig. 13). The increase in precipitation over the Sahel is not being supplied by flow off the Gulf of Guinea, but from the west. This westerly flow enhancement is similar to a mode of variability seen in the present-day climatology. Grist and Nicholson (2001) find that in years when the Sahel region receives more precipitation, the low-level westerly winds near 10°–15°N are stronger. However, in the present-day climatology this variability mechanism is not associated with warming in the Gulf of Guinea.

There is also some similarity with the African Humid Period (AHP). About 6000 yr ago, when summer insolation at 15°N was about 5% greater than today due to differences in the precession of the earth's orbit, the Sahel and even the Sahara received enough precipitation to support savanna vegetation and wildlife (e.g., Hoelzmann et al. 1998). According to the regional climate model simulations of Patricola and Cook (2005, manuscript submitted to *J. Climate*), the primary source of anomalous moisture north of about 15°N was not flow off the Gulf of Guinea, but westerly flow from the subtropical Atlantic. The high climatological precipitation north of about 15°N was maintained when low-level relative vorticity increases (stretching) associated with midtropospheric condensational heating were balanced by the advection of low relative vorticity

air from the Atlantic high. (In today's West African monsoon, the primary balance is the Sverdrup balance, in which low *planetary* vorticity air from over the Gulf of Guinea flows northward to balance the low-level stretching and maintain the system.) A strengthening and deepening of the low-level westerly jet onto the west coast of Africa accomplishes the transport of low relative vorticity air from the subtropical high, and brings additional moisture to the Sahel and southern Sahara during the AHP. However, in the AHP case, this response is associated with warming of the land surface at these latitudes due to solar forcing, not warming of the Gulf of Guinea.

This behavior of the MIROC(medres) simulation under the A2 forcing bears similarity to known modes of variability of the West African monsoon, and this model produced one of the best simulations of the twentieth-century climate in West Africa. But the suddenness of the warming in the Gulf of Guinea, and its large magnitude, seems unreasonable for so early in the twenty-first century. Perhaps the MIROC(medres) simulations are offering a view of the twenty-second century or beyond, if greenhouse gas emissions continue unchecked.

Under the A2 greenhouse gas scenario, the MRI integration produces more frequent dipole events, with the number of events greater during the second half of the century than during the first half. Compared with 12 dry Sahel/wet Guinean coast years in the second half of the twentieth-century integration, the MRI model produces 15 dry/wet years in the first half of the twenty-first century, and 20 events in the second half. (These are ensemble means.) Only the frequency of dry Sahel/wet Guinean coast increases, not the magnitude of the anomaly. The dynamics of the dipole precipitation anomaly is the same as in the twentieth-century integrations, including an enhancement of the midtropospheric northerly outflow from the Saharan high.

Figures 14a,b show precipitation anomalies for the first 20 yr of the twenty-first century under the A2 and B1 greenhouse gas–forcing scenarios, respectively. The anomalies are differences from the twentieth-century precipitation climatology in the MRI model, and all five ensemble members are averaged. Modest precipitation increases along the Guinea coast are present in both scenarios, and they are somewhat more widespread under the A2 scenario. There is no drying in the Sahel under either scenario.

Sahelian drying begins to emerge in the middle of the twenty-first century in the integration with the A2 forcing scenario (Fig. 14c). Wet conditions along the Guinean coast strengthen, and the southerly flow anomaly in the midtroposphere that leads to subsidence over the Sahel in induced. In the B1 scenario (Fig. 14d), with much less greenhouse gas loading of the atmosphere, drying over the Sahel is not apparent.

In the last 20 yr of the twenty-first century, the A2 scenario brings greater drying across the Sahel. These precipitation decreases are on the order of 10% of the annual mean near 10°N (see Fig. 2). Drying is especially strong on the west coast (over Senegal, Guinea-Bissau, the Gambia, Sierra Leone, and Guinea) and inland over northern Nigeria and southern Niger. Under the B1 scenario, there is still no notable drying across the Sahel even by the end of the century, but it seems that a pattern similar to that of the A2 scenario case is emerging.

5. Conclusions

Coupled GCM simulations of the second half of the twentieth century are examined to evaluate the accuracy with which these models capture the climatology and one prominent mode of interannual variability of the West African summer monsoon. This assessment is used to select models for the analysis of twenty-first-century projections of the West African monsoon under various greenhouse gas–forcing scenarios. Such an approach is useful when there is no consensus among the models' projections of future climate on which we can build confidence in (or a statistical analysis of) the predictions.

Overall, the current generation of coupled GCMs is much more capable of accurately representing the summer precipitation climatology over North America and Europe than over Africa. Eight of the 18 simulations examined fail to capture the West African monsoon system in the sense that they do not place a precipitation maximum over the African land surface. Instead, the strongest precipitation remains over the Gulf of Guinea to the south of the coast in these simulations.

In today's climate, warm SSTAs of 1 K or smaller are associated with a precipitation dipole anomaly that features dry conditions in the Sahel and wet conditions along the Guinean coast. Since the dynamics of this mode of variability is understood, it provides a good opportunity to evaluate one physical process of interannual variability in the coupled models, and helps us develop some perspective on the models' ability to simulate climate change in this region. Six of the 10 coupled GCM integrations that produce a West African monsoon (over the land) also capture the dipole variability mode with some degree of accuracy, including reasonable intensities and recurrence frequencies as well as the physical processes.

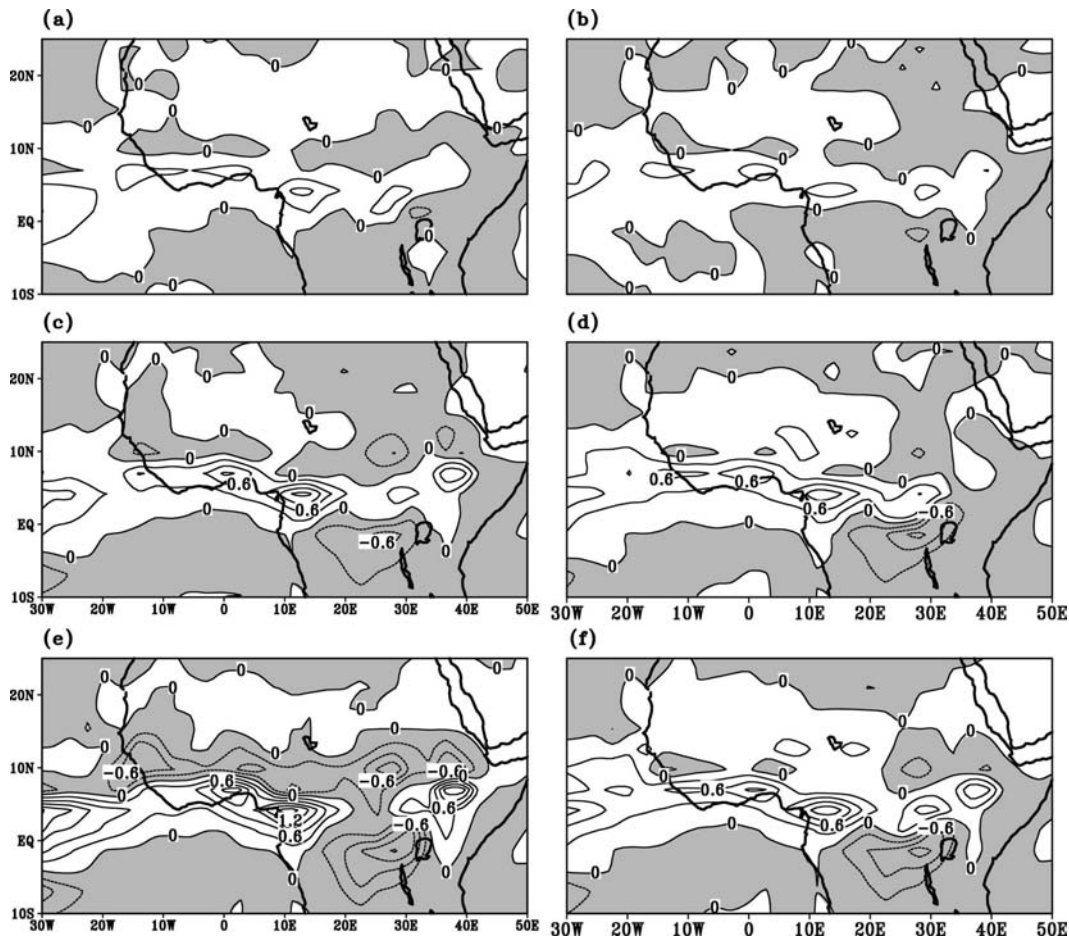Simulations of the twenty-first century from three

FIG. 14. JJAS precipitation differences (mm day^{-1}) from the 1949–2000 mean from the MRI model for (a) the 2001–20 A2 scenario mean, (b) the 2001–20 B1 scenario mean, (c) the 2041–60 A2 scenario mean, (d) the 2041–60 A2 scenario mean, (e) the 2081–2100 A2 scenario mean, and the (f) the 2081–2100 B1 scenario mean.

coupled GCM integrations, selected for their reasonable simulations of the twentieth-century climate, are examined in detail under various assumptions about how greenhouse gas emissions may change in the future. These model simulations are referred to as GFDL_0, MIROC(medres), and MPI (see Table 2). Perversely, the three selected models all behave differently under twenty-first-century greenhouse gas forcing. Under the rather severe A2 forcing scenario, the Sahel in GFDL_0 begins to dry around the middle of the twenty-first century and the drying spreads to the Guinean coast region and essentially disables the West African monsoon system by the end of the century. Because there is a significant inaccuracy in this model's simulation of the present-day climatology, with northward instead of southward flow in the midtroposphere over the Sahel near the Greenwich meridian, and extreme surface warming with no analog in the present-day climatology, this may not be the most plausible

projection of future climate available from the suite of coupled GCMs examined here.

In the MIROC(medres) integrations of the twenty-first century, strong warming in the Gulf of Guinea reverses meridional geopotential height gradients across the Guinean coast, stopping the northward monsoon flow across the Guinean coast and greatly reducing summer precipitation for the Guinean coast countries. Westerly flow onto the continent near 15°N is enhanced, resulting in a substantial *increase* in Sahel precipitation rates. This model is exhibiting a threshold response to localized 2-K warming in the Gulf of Guinea, which disrupts the West African monsoon when geopotential heights over the ocean fall below those of the land in summer. Because the SSTAs are so strong, and the warming happens quite suddenly in the very beginning of the twenty-first century in the model, this might not be the most reliable prediction for the coming decades. However, the MIROC model pro-

duces one of the best (along with the MRI model) simulations of the present-day climatology and its variability, and the atmosphere's response to the strong Gulf of Guinea SSTAs seems reasonable. This model may be providing insight into a future response, perhaps for the twenty-second century if Gulf of Guinea SSTAs exceed 2 K under greenhouse gas forcing.

A third model, from MRI, has a more modest increase in Gulf of Guinea SSTs in the twenty-first-century integrations. Under each greenhouse gas–forcing assumption examined, the Sahel receives less precipitation and the Guinean coast receives more in the second half of the twenty-first century. The dynamics of this response is consistent with the response to warm Gulf of Guinea SSTs in the present-day climate. The changes in precipitation do not occur as a smooth trend, but as an increase in the number of years in the number of dry years in the Sahel. This pattern of precipitation changes has implications for impacts analyses, since the occurrence of more dry years in the Sahel has different and, perhaps, more severe repercussions than an overall small decrease in precipitation would have.

The analysis indicates that the MRI simulations are most likely providing the most reliable simulation of twenty-first-century climate over West Africa. According to these model integrations, by the end of the twenty-first century, with a continuation of the present-day increases in the rate of greenhouse gas emissions assumed in the A2 scenario, the number of dry years in the Sahel will approximately double, leading to a decrease of about 10% in the summer precipitation climatology. Precipitation rates along the Guinean coast will increase by about 10%. Under the assumptions of the B1 scenario, drying in the Sahel is postponed beyond the twenty-first century, but there are precipitation increases of about 1 mm day^{-1} over the Guinean coast by the end of the century.

The analysis of the atmospheric dynamics indicates that increases in precipitation along the Guinean coast in response to warm SSTs in the Gulf of Guinea are captured more reliably and completely in GCMs than the attendant drying in the Sahel. Thus, the MRI simulations could be underestimating the degree of drying in the Sahel in the future climate simulations.

Changes associated with warming in the Gulf of Guinea are isolated in this study to allow a physically based analysis of the model simulations; the full complexity of the West African monsoon system and its variability is not considered. Other forcing mechanisms are known to be important and will also contribute to trends in Sahelian rainfall. These need to be better understood. One example is warming in the Indian Ocean, which is observed in the late twentieth century and may be related to a drying trend in the Sahel. However, none of these models captures the observed twentieth-century drying trend in the Sahel in their ensemble means. In the twenty-first-century integrations, each of the GCM integrations examined has a pronounced warming trend in the Indian Ocean. The implications of this Indian Ocean warming for African precipitation require further investigation.

REFERENCES

Cook, K. H., 1997: Large-scale atmospheric dynamics and Sahelian precipitation. *J. Climate,* **10,** 1137–1152.

Druyan, L. M., 1991: The sensitivity of Sub-Saharan precipitation to Atlantic SST. *Climate Change,* **18,** 17–36.

Folland, C. K., J. A. Owen, M. N. Ward, and A. W. Colman, 1991: Prediction of seasonal rainfall in the Sahel region of Africa using empirical and dynamical methods. *J. Forecasting,* **10,** 21–56.

Gadgil, S., and S. Sajani, 1998: Monsoon precipitation in the AMIP runs. *Climate Dyn.,* **14,** 659–689.

Grist, J. P., and S. E. Nicholson, 2001: A study of the dynamic factors influencing rainfall variability in the West African Sahel. *J. Climate,* **14,** 1337–1359.

Hastenrath, S., 1984: Interannual variability and annual cycle: Mechanisms of circulation and climate in the tropical Atlantic sector. *Mon. Wea. Rev.,* **112,** 1097–1107.

Hoelzmann, P., D. Jolly, S. P. Harrison, F. Laarif, R. Bonnefille, and H. J. Pachur, 1998: Mid-Holocene land-surface conditions in northern Africa and the Arabian Peninsula: A data set for the analysis of biogeophysical feedbacks in the climate system. *Global Biogeochem. Cycles,* **12,** 35–51.

Houghton, J. T., Y. Ding, D. J. Griggs, M. Noguer, P. J. van der Linden, and D. Xiaosu, Eds., 2001: *Climate Change 2001: The Scientific Basis.* Cambridge University Press, 944 pp.

Huffman, G. J., and Coauthors, 1997: The Global Precipitation Climatology Project (GPCP) combined precipitation data set. *Bull. Amer. Meteor. Soc.,* **78,** 5–20.

Janicot, S., 1992: Spatiotemporal variability of West African rainfall. Part II: Associated surface and airmass characteristics. *J. Climate,* **5,** 499–511.

Janowiak, J. E., 1988: An investigation of interannual rainfall variability in Africa. *J. Climate,* **1,** 240–255.

Kalnay, E., and Coauthors, 1996: The NCEP/NCAR 40-Year Reanalysis Project. *Bull. Amer. Meteor. Soc.,* **77,** 437–471.

Lamb, P. J., 1978a: Case studies of tropical Atlantic surface circulation patterns during recent sub-Saharan weather anomalies: 1967 and 1968. *Mon. Wea. Rev.,* **106,** 482–491.

——, 1978b: Large-scale tropical Atlantic surface circulation patterns associated with sub-Saharan weather anomalies. *Tellus,* **30,** 240–251.

——, and R. A. Peppler, 1992: Further case studies of tropical Atlantic surface atmospheric and oceanic patterns associated with sub-Saharan drought. *J. Climate,* **5,** 476–488.

Lough, J. M., 1986: Tropical Atlantic sea surface temperatures and rainfall variations in sub-Saharan Africa. *Mon. Wea. Rev.,* **114,** 561–570.

Meehl, G. A., and C. Tebaldi, 2004: More intense, more frequent, and longer lasting heat waves in the 21st century. *Science,* **305,** 994–997.

New, M., M. Hulme, and P. Jones, 1999: Representing twentieth-century space-time climate variability. Part I: Development of a 1961-1990 mean monthly terrestrial climatology. *J. Climate,* **12,** 829–856.

Nicholson, S. E., 1980: The nature of rainfall fluctuations in subtropical West Africa. *Mon. Wea. Rev.,* **108,** 473–487.

——, and I. M. Palao, 1993: A re-evaluation of rainfall variability in the Sahel. Part I: Characteristics of rainfall fluctuations. *Int. J. Climatol.,* **4,** 371–389.

——, B. Some, and B. Kone, 2000: An analysis of recent rainfall conditions in West Africa, including the rainy seasons of the 1997 El Niño and the 1998 La Niña years. *J. Climate,* **13,** 2628–2640.

Reynolds, R. W., and T. M. Smith, 1994: Improved global sea surface temperature analysis. *J. Climate,* **7,** 929–948.

Rowell, D. P., C. K. Folland, K. Maskell, and M. N. Ward, 1995: Variability of summer rainfall over tropical north Africa (1906-92): Observations and modelling. *Quart. J. Roy. Meteor. Soc.,* **121,** 669–704.

Semazzi, F. H. M., V. Mehta, and Y. C. Sud, 1988: An investigation of the relationship between sub-Saharan rainfall and global sea surface temperatures. *Atmos.–Ocean,* **26,** 118–138.

Vizy, E. K., and K. H. Cook, 2001: Mechanisms by which Gulf of Guinea and eastern North Atlantic sea surface temperature anomalies can influence African rainfall. *J. Climate,* **14,** 795–821.

——, and ——, 2002: Development and application of a mesoscale climate model for the tropics: Influence of sea surface temperature anomalies on the West African monsoon. *J. Geophys. Res.,* **107,** 4023, doi:10.1029/2001JD000686.

Ward, M. N., 1998: Diagnosis and short-lead time prediction of summer rainfall in tropical North Africa at interannual and multidecadal timescales. *J. Climate,* **11,** 3167–3191.

Xie, P., and P. A. Arkin, 1997: Global precipitation: A 17-year monthly analysis based on gauge observations, satellite estimates, and numerical model outputs. *Bull. Amer. Meteor. Soc.,* **78,** 2539–2558.